ELSEVIER

Journal of Alloys and Compounds 317–318 (2001) 120–126

Journal of ALLOYS AND COMPOUNDS

www.elsevier.com/locate/jallcom

Synthesis, crystal structure and TEM study of the new hollandite-type $Ba_{\sim 8/7}Mo_8O_{16}$

N. Barrier[a,*], P. Gougeon[a], R. Retoux[b]

[a]*Laboratoire de Chimie du Solide et Inorganique Moléculaire, U.R.A. C.N.R.S. n° 1495, Université de Rennes I, Avenue du Général Leclerc, 35042 Rennes Cedex, France*

[b]*Laboratoire des Fluorures, UPRES-A CNRS 6010, Université du Maine, 72085 Le Mans Cedex 9, France*

Abstract

Investigation of the Cs–Ba–Mo–O system by fused salt electrolysis at 960°C has led to the new related-hollandite compound $Ba_{\sim 8/7}Mo_8O_{16}$. Single-crystals of $Ba_{\sim 8/7}Mo_8O_{16}$ were examined by electron diffraction and high-resolution electron microscopy. $Ba_{\sim 8/7}Mo_8O_{16}$ was found to present a tetragonal I basic unit-cell (a=10.21 Å, c=2.89 Å) with a one-dimensional modulation of wavevector **q** close to 4/7 along c^* at room temperature. Refinement of the crystal structure was made on X-ray single crystal data in the seven-fold supercell in the three-dimensional space group *I4* (a=10.214(2) Å, c=20.255(5) Å, $R_w(F^2)$=0.0844 for all 7767 independent reflections and 149 parameters). In the latter supercell approach, the Mo atoms in the double edge-sharing rutile-type chains form Mo_3 triangles and planar rhomboidal Mo_4 clusters that coexist in equal proportions. The Mo–Mo distances vary from 2.5341(8) to 2.696(2) Å and from 2.5341(8) to 2.894(4) Å in the Mo_3 and Mo_4 clusters, respectively. The shortest intercluster distance is 3.047(4) Å. The Mo–O distances range between 1.81(1) to 2.418(8) Å as usually observed in reduced molybdenum oxides. The Ba^{2+} cations occupy the large square channels in square prismatic environment of oxygen atoms with the distribution sequence ...Ba–□–Ba–Ba–□Ba–□–....

Keywords: Hollandite; Barium; Molybdenum; Oxide; Clusters; TEM studies

1. Introduction

Since the report of the crystal structure of the mineral hollandite $Ba_xMn_8O_{16}$ (x ~0.96) by Byström and Byström in 1950 [1], a large number of ternary transition-metal oxides $A_xM_8O_{16}$ (A=K, Rb, Cs, Ba, Pb ...; M=Ti, V, Cr, Mn, Fe, Mo, Ru ...) which crystallize in the hollandite-type structure have been synthesized by solid state reaction or fused-salt electrolysis. Most of these studies were motivated by the possible use of the hollandite-type compounds as nuclear waste immobilizers, solid state electrolytes or fast ionic conductors [2]. Most importantly, these phases frequently exhibit complex commensurate or incommensurate superstructures due to partial occupation and ordering of the A cation within the four-sided tunnels [3]. Indeed, the hollandite structure consists of double rutile chains sharing edges and corners of the MO_6 octahedra to form one-dimensional four-sided tunnels of 2×2 octahedra in cross section, often noted T(2,2), in which the A cations reside as well as empty smaller tunnels having 1×1 octahedron in cross section (T(1,1) tunnels). Reduced molybdenum oxides which crystallize with a hollandite-type structure constitute an interesting subgroup. Indeed, the Mo atoms form Mo–Mo bonds which manifest as tetrameric rhomboidal Mo_4 clusters in $K_2Mo_8O_{16}$ [4] and $Ba_{1.14}Mo_8O_{16}$ [5] synthesized by solid state reaction, and Mo_3 triangles either isolated or forming infinite chains in $La_{1.16}Mo_8O_{16}$ [6] and $NdMo_6O_{12}$ (i.e. $Nd_{1.33}Mo_8O_{16}$) [7], respectively, obtained by fused-salt electrolysis. We report here the synthesis, the electron microscopy study and the single-crystal structure determination of a new reduced ternary oxide of molybdenum which adopts the hollandite-type structure: $Ba_{\sim 8/7}Mo_8O_{16}$.

2. Experimental section

2.1. Synthesis

The starting reagents used in this synthesis were Cs_2MoO_4, $BaMoO_4$, MoO_3 (Strem, 99.9%). Caesium and barium molybdates were prepared by reacting Cs_2CO_3 and

*Corresponding author.

0925-8388/01/$ – see front matter
PII: S0925-8388(00)01325-6

$BaCO_3$ (Strem, 99.9%), respectively, with a stoichiometric amount of MoO_3 at 600°C and 800°C overnight. MoO_3 was annealed in air at 400°C before use. Single crystals of $Ba_{\sim 8/7}Mo_8O_{16}$ were obtained by the electrolysis of a melt formed at 960°C from a mixture of Cs_2MoO_4, MoO_3 and $BaMoO_4$ having the molar ratio 5.2:1.5:2. The electrolysis was carried out in air using an high-purity alumina crucible. The anode was a Pt foil with a surface area of about 1 cm^2 and the cathode a 10 turn Pt spiral of about 1 cm long made from a 0.4 mm-diameter wire. At the end of the process, the electrodes were raised above the melt to allow them to cool rapidly to room temperature. Crystals which grow perpendicularly to the cathode in the form of black needle shaped square prisms with the needle axis parallel to the tetragonal *c*-axis (max. dimensions $0.8\times 0.8\times 5$ mm^3) were obtained by applying a constant current of 36 mA for 12 h. Single crystals were separated from the matrix and the cathode by repeated and alternate washings in hot dilute solutions of potassium carbonate and hydrochloric acid.

2.2. Structure determination

A needle-like crystal of approximate dimensions $0.28\times 0.028\times 0.027$ mm^3 was selected for data collection. Intensity data were collected on a Nonius Kappa CCD diffractometer using a graphite-monochromatized MoKα radiation ($\lambda = 0.71073$ Å) at room temperature. The frames were recorded using $\Delta\omega = 2°$ rotation scans with an X-ray exposure time of 60 s. Reflection indexing, Lorentz-polarization correction, peak integration and background determination were performed using the program DENZO of the Kappa CCD software package [8]. An empirical absorption correction was applied with the SORTAV program [9]. Examination of the data set did not show any supplementary systematic extinctions other than that corresponding to the I-type lattice and revealed that the Laue class was 4/m leading to space groups *I4*, $I\bar{4}$ or *I4*/*m*. The structure was solved by direct methods using SHELXS [10] and subsequent difference Fourier syntheses in space group *I4*. All structure refinements and Fourier syntheses

Table 1
Crystallographic and experimental data for $Ba_{\sim 8/7}Mo_8O_{16}$

Formula	$Ba_{\sim 8/7}Mo_8O_{16}$
Molecular mass	1180.48
Crystal system	tetragonal
Space group	*I4*
a(Å)	10.2160(5)
c(Å)	20.2449(8)
V(Å)	2112.9(2)
Z	7
Density (calc., $g.cm^{-3}$)	6.494
Temperature (K)	293
Diffractometer	Nonius Kappa CCD
Radiation	MoKα radiation ($\lambda = 0.71073$Å)
Crystal color	black
Morphology	needle
Crystal size (mm^3)	$0.28\times 0.028\times 0.027$
Linear absorption coeff. (mm^{-1})	11.78
Monochromator	Oriented graphite
Scan mode	1° $\Delta\omega$ scan
Recording range 20 (°)	4–90.4
hkl range	−20/17, −18/20, −40/27
No. of measured reflections	28 718
No. of independent reflections	7767
No. of observed reflections with $F^2 > 2$ $\sigma(F^2)$	4591
R_{int}	0.052
Absorption correction	Sortav[9]
Transmission (min.–max.)	0.260–0.747
Refinement	F^2
Calculated weights	$w = l/[\sigma^2(Fo^2) + (0.0571P)^2 + 0.7462P]$ where $P = (Fo^2 + 2Fc^2)/3$
Extinction coefficient	0.00026(3)
*R*1, *wR*2 [$F^2 > 2\ \sigma(F^2)$]	0.0444, 0.1153
*R*1, *wR*2 on all data	0.0844, 0.1401
S	1.079
No. of refined parameters	149
$\Delta\rho$ min, max. ($e.Å^{-3}$)	−3.478, 3.620

Table 2
Atomic coordinates ($\times 10^4$) and equivalent isotropic displacement parameters ($Å^2 \times 10^3$) for $Ba_{\sim 8/7}Mo_8O_{16}$

	X	Y	Z	U(eq)[a]
Ba(1)	5000	5000	3619(1)	16(1)
Ba(2)	0	0	6852(3)	11(1)
Ba(3)	0	0	5890(1)	20(1)
Ba(4)	0	0	4090(2)	21(1)
Ba(5)	0	0	3172(2)	15(1)
Ba(6)	0	0	1353(1)	21(1)
Ba(7)	0	0	490(20)	60(14)
Mo(1)	1493(1)	3284(1)	5642(1)	9(1)
Mo(2)	3231(1)	1829(1)	5009(1)	12(1)
Mo(3)	1548(2)	3268(1)	4391(1)	13(1)
Mo(4)	1494(2)	3267(2)	8487(1)	10(1)
Mo(4′)	1485(2)	3272(2)	8717(2)	7(1)
Mo(5)	3360(2)	17763(1)	7824(1)	13(1)
Mo(6)	1721(1)	3192(1)	7201(1)	10(1)
Mo(7)	3506(1)	1725(1)	6558(1)	9(1)
O(1)	1557(8)	1955(8)	6419(3)	8(1)
O(2)	1693(10)	4587(10)	6447(5)	13(2)
O(3)	3319(10)	425(9)	5748(4)	12(1)
O(4)	3497(10)	3129(10)	5755(4)	20(2)
O(5)	1662(5)	4736(5)	5011(6)	12(1)
O(6)	1221(4)	1710(4)	4991(4)	11(1)
O(7)	−403(9)	3327(9)	4306(4)	10(1)
O(8)	3489(7)	3117(7)	4280(3)	11(1)
O(9)	3294(5)	408(5)	8594(6)	10(1)
O(10)	3477(6)	3039(6)	8611(4)	11(1)
O(11)	1672(10)	4657(9)	7875(5)	13(2)
O(12)	1312(7)	1696(7)	7831(3)	15(1)
O(13)	3343(8)	295(8)	7170(4)	9(1)
O(14)	3712(8)	3280(8)	7175(4)	15(1)

[a] U_{eq} is defined as one third of the trace of the orthogonalized U_{ij} tensor.

were carried out using SHELXL-97 [11]. Full-matrix least-squares refinement of a model based on seven Ba, six Mo and fourteen O atoms on F^2 with anisotropic atomic displacement parameters for the Ba and Mo atoms and occupancy factors for the Ba atoms converged to a residual $R(F_0^2)=0.065$ for the 4591 reflections having $F_0^2 > 2\sigma(F_0^2)$ with a positive residual electron density $\Delta\rho=6.2$ e.A^{-3}. However, the isotropic atomic displacement parameter of Mo4 was about three time higher than those of the other Mo atoms. Consequently, the Mo4 position was split in two positions Mo4 and Mo4′ and their occupancy factor were allowed to be refined. Refinement of the latter model lowered the R value to 0.0444 and the maximum electron density residue to 3.62 e.A^{-3}. Refinements of the occupancy factors for the Mo sites yielded values of 0.71(1) and 0.29(1) for the Mo4 and Mo4′ sites respectively and showed that the remaining Mo sites were fully occupied. The total occupancy number of Ba atoms corresponded to the formula $Ba_{\sim 8/7}Mo_8O_{16}$ within the e.s.d. equal to 0.01. It is interesting to note that the stoichiometry in barium corresponds to 2q as previously observed in incommensurate modulated hollandite-type structure [12]. Some data collection and refinement parameters are given in Table 1. The final values of the positional parameters, isotropic-equivalent atomic displacement parameters and their stan-

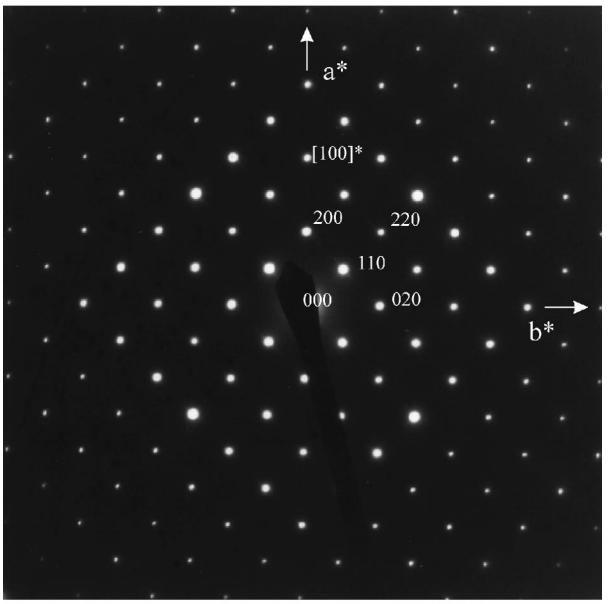

(a)

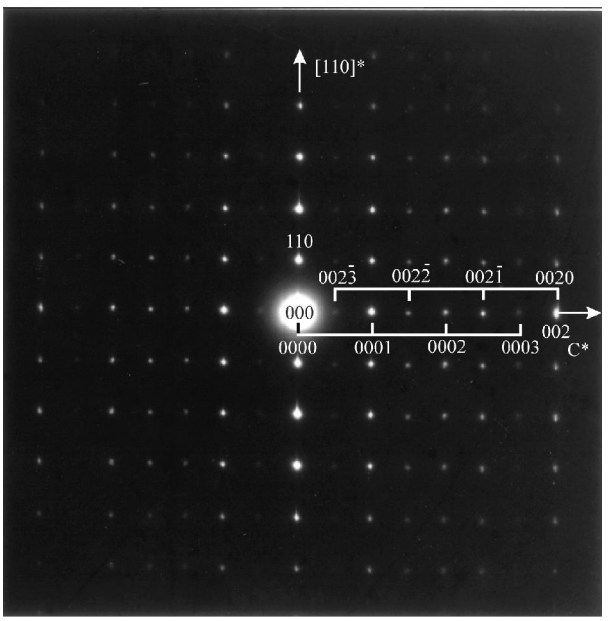

(b)

Fig. 1. Electron diffraction pattern of $Ba_{\sim 8/7}Mo_8O_{16}$ along [001]* (a) and [1−10]* (b) of the tetragonal unit cell. In (b) the extra spots are indexed with a four indices notation where the fourth number is related to the order of satellite of an intense spot of the main cell.

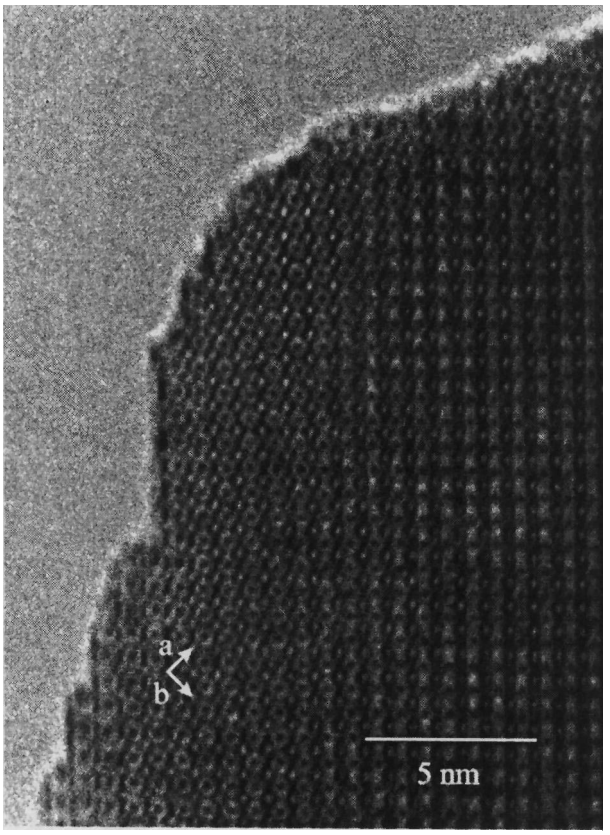

Fig. 2. HREM image along the [001] zone showing the absence of planar defects.

dard uncertainties are reported in Table 2. Selected interatomic distances and anisotropic displacement parameters are presented in Tables 3 and 4, respectively.

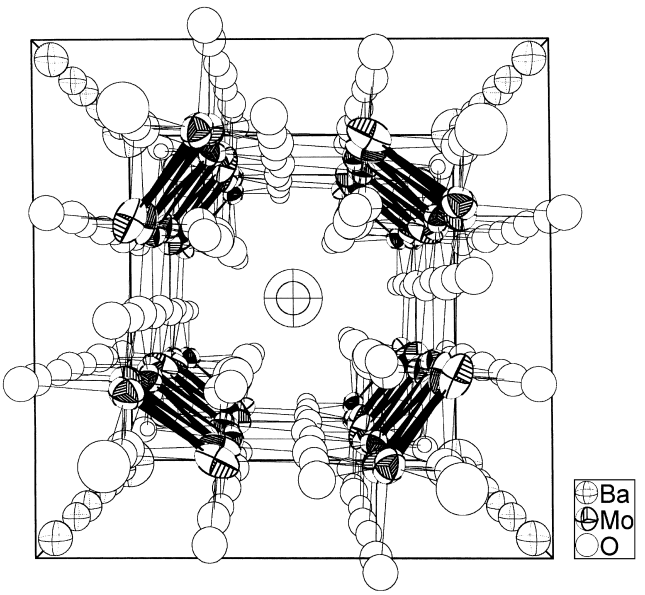

Fig. 3. View of the $Ba_{\sim 8/7}Mo_8O_{16}$ structure along the tetragonal *c*-axis. Displacement ellipsoids are drawn at the 97% of probability level.

Table 3
Selected interatomic distances for $Ba_{\sim 8/7}Mo_8O_{16}$ [a]

Ba(1)–O(12)≠l	2.710(7)
Ba(1)–O(12)≠2	2.710(7)
Ba(1)–O(12)≠3	2.710(7)
Ba(1)–O(12)≠4	2.710(7)
Ba(1)–O(8)≠5	2.807(7)
Ba(1)–O(8)	2.807(7)
Ba(1)–O(8)≠6	2.807(7)
Ba(1)–O(8)≠7	2.807(7)
Ba(2)–O(1)≠8	2.700(8)
Ba(2)–O(1)≠9	2.700(8)
Ba(2)–O(1)	2.700(8)
Ba(2)–O(1)≠10	2.700(8)
Ba(2)–O(12)	2.954(8)
Ba(2)–O(l 2)≠9	2.954(8)
Ba(2)–O(12)≠10	2.954(8)
Ba(2)–O(12)≠8	2.954(8)
Ba(2)–Ba(1)≠11	3.577(6)
Ba(3)–O(1)	2.769(8)
Ba(3)–O(1)≠9	2.769(8)
Ba(3)–O(1)≠10	2.769(8)
Ba(3)–O(1)≠8	2.769(8)
Ba(3)–O(6)≠8	2.815(7)
Ba(3)–O(6)≠9	2.815(7)
Ba(3)–O(6)≠10	2.815(7)
Ba(3)–O(6)	2.815(7)
Ba(3)–Ba(4)	3.644(2)
Ba(4)–O(10)≠1	2.715(6)
Ba(4)–O(10)≠12	2.715(6)
Ba(4)–O(10)≠13	2.715(6)
Ba(4)–O(10)≠14	2.715(6)
Ba(4)–O(6)	2.817(7)
Ba(4)–O(6)≠9	2.817(7)
Ba(4)–O(6)≠10	2.817(7)
Ba(4)–O(6)≠8	2.817(7)
Ba(5)–O(10)≠1	2.687(6)
Ba(5)–O(10)≠13	2.687(6)
Ba(5)–O(10)≠14	2.687(6)
Ba(5)–O(10)≠12	2.687(6)
Ba(5)–O(14)≠12	2.981(8)
Ba(5)–O(14)≠1	2.981(8)
Ba(5)–O(14)≠13	2.981(8)
Ba(5)–O(14)≠14	2.981(8)
Ba(5)–Ba(6)	3.683(4)
Ba(6)–O(4)≠12	2.734(10)
Ba(6)–O(4)≠1	2.734(10)
Ba(6)–O(4)≠13	2.734(10)
Ba(6)–O(4)≠14	2.734(10)
Ba(6)–O(14)≠1	2.755(8)
Ba(6)–O(14)≠13	2.755(8)
Ba(6)–O(14)≠12	2.755(8)
Ba(6)–O(14)≠14	2.755(8)
Ba(7)–O(4)≠1	2.509(13)
Ba(7)–O(4)≠13	2.509(13)
Ba(7)–O(4)≠12	2.509(13)
Ba(7)–O(4)≠14	2.509(13)
Ba(7)–Ba(1)≠12	3.79(4)
Mo(1)–O(5)	1.966(8)
Mo(1)–O(3)≠10	1.972(9)
Mo(1)–O(4)	2.066(10)

Table 3. Continued

Mo(1)–O(1)	2.078(7)
Mo(1)–O(6)	2.097(6)
Mo(1)–O(2)	2.115(10)
Mo(1)–Mo(3)	2.5341(8)
Mo(1)–Mo(2)	2.6465(18)
Mo(1)–Mo(6)	3.1668(17)
Mo(1)–Mo(7)	3.1938(11)
Mo(2)–O(8)	1.993(6)
Mo(2)–O(4)	2.030(9)
Mo(2)–O(7)≠9	2.039(9)
Mo(2)–O(6)	2.058(4)
Mo(2)–O(3)	2.075(9)
Mo(2)–O(5)≠6	2.083(5)
Mo(2)–Mo(3)	2.5847(15)
Mo(2)–Mo(4′)≠1	2.633(5)
Mo(2)–Mo(4)≠1	3.095(3)
Mo(2)–Mo(7)	3.151(2)
Mo(3)–O(5)	1.960(8)
Mo(3)–O(7)	2.002(9)
Mo(3)–O(8)	2.001(7)
Mo(3)–O(6)	2.029(6)
Mo(3)–O(10)≠1	2.068(8)
Mo(3)–O(9)≠1	2.111(9)
Mo(3)–Mo(4′)≠1	2.894(4)
Mo(3)–Mo(4)≠1	3.131(3)
Mo(3)–Mo(5)≠1	3.1732(12)
Mo(4)–O(11)	1.893(10)
Mo(4)–O(9)≠10	1.956(6)
Mo(4)–O(10)	2.055(6)
Mo(4)–O(12)	2.092(7)
Mo(4)–O(8)≠16	2.140(7)
Mo(4)–O(7)≠17	2.151(9)
Mo(4)–Mo(6)	2.614(3)
Mo(4)–Mo(5)	2.786(3)
Mo(4)–Mo(2)≠16	3.095(3)
Mo(4)–Mo(3)≠16	3.131(3)
Mo(4′)–O(7)≠17	1.813(10)
Mo(4′)–O(8)≠16	1.821(7)
Mo(4′)–O(9)≠10	1.950(6)
Mo(4′)–O(10)	2.061(6)
Mo(4′)–O(11)	2.223(10)
Mo(4′)–O(12)	2.418(8)
Mo(4′)–Mo(2)≠16	2.633(5)
Mo(4′)–Mo(3)≠16	2.894(4)
Mo(4′)–Mo(5)	3.047(4)
Mo(4′)–Mo(6)	3.079(5)
Mo(5)–O(13)	2.009(9)
Mo(5)–O(11)≠6	2.031(10)
Mo(5)–O(14)	2.056(8)
Mo(5)–O(10)	2.055(7)
Mo(5)–O(9)	2.093(9)
Mo(5)–O(12)	2.093(7)
Mo(5)–Mo(6)	2.5481(9)
Mo(5)–Mo(7)	2.5678(16)
Mo(5)–Mo(3)≠16	3.1732(12)
Mo(6)–O(11)	2.025(10)
Mo(6)–O(1)	2.034(7)
Mo(6)–O(12)	2.034(7)
Mo(6)–O(14)	2.037(8)
Mo(6)–O(13)≠10	2.066(8)
Mo(6)–O(2)	2.088(10)
Mo(6)–Mo(7)	2.696(2)

Table 3. Continued

Mo(7)–O(13)	1.923(8)
Mo(7)–O(2)≠6	1.962(10)
Mo(7)–O(1)	2.024(8)
Mo(7)–O(14)	2.032(8)
Mo(7)–O(3)	2.119(9)
Mo(7)–O(4)	2.168(9)

[a] Symmetry transformations used to generate equivalent atoms: ≠1 $-x+1/2, -y+1/2, z-1/2$; ≠2 $y+1/2, -x+1/2, z-1/2$; ≠3 $-y+1/2, x+1/2, z-1/2$; ≠4 $x+1/2, y+1/2, z-1/2$; ≠5 $-x+1, -y+1, z$; ≠6 $-y+1, x, z$; ≠7 $y, -x+1, z$; ≠8 $-x, -y, z$; ≠9 $y, -x, z$; ≠10 $-y, x, z$; ≠11 $x-1/2, y-1/2, z+1/2$; ≠12 $x-1/2, y-1/2, z-1/2$; ≠13 $-y+1/2, x-1/2, z-1/2$; ≠14 $y-1/2, -x+1/2, z-1/2$; ≠15 $x+1/2, y+1/2, z+1/2$; ≠16 $-x+1/2, -y+1/2, z+1/2$; ≠17 $-y+1/2, x+1/2, z+1/2$.

2.3. Transmission electron microscopy studies

The High Resolution Electron Microscopy (HREM) and Electron Diffraction (ED) studies were performed on a 200 KV side entry JEOL 2010 electron microscope (tilt±30°). The chemical composition of the samples was confirmed using an Energy Dispersive X-ray analysis (EDX) done with a KEVEX EDX spectrometer. Thin crystals were crushed in an agate mortar and suspended in alcohol and a few droplets of the suspension were put on a carbon coated holey film to prepare the specimen for electron microscopy.

3. Results and discussion

3.1. Electron diffraction and high resolution electron microscopy studies

Reciprocal lattice reconstructions performed in the ED study showed that the intense spots can be indexed in a tetragonal I main cell with lattice parameters $a \sim 10.2$ Å and $c \sim 2.9$ Å. Fig. 1a,b present the electron diffraction patterns obtained along the [001]* and [1−10]* zone axis. In Fig. 1b extra spots in incommensurate position are clearly visible along the *c*-axis on the diffraction patterns. The modulation wavevector q deduced from careful measurements on these electron diffraction patterns is close to 4/7. In Fig. 1b the extra spots are indexed with a four indices notation where the fourth number is related to the order of satellite of a intense spot of the main cell. The [001] HREM image presented Fig. 2 exhibits a typical contrast observed in this oxide. The regular contrasts observed on large zones suggests that this compound is a quite well ordered phase if the structure is seen along the *c*-axis. In particular, we did not observe planar defects such as crystallographic shear planes leading to larger rectangular (e.g. 3×2 octahedra) channels as encountered in the mineral hollandite [13].

Table 4
Anisotropic displacement parameters ($Å^2 \times 10^3$) for 1[a]

	U11	U22	U33	U23	U13	U12
Ba(1)	12(1)	12(1)	25(1)	0	0	0
Ba(2)	9(1)	9(1)	16(2)	0	0	0
Ba(3)	12(1)	12(1)	37(1)	0	0	0
Ba(4)	12(1)	12(1)	39(1)	0	0	0
Ba(5)	13(1)	13(1)	19(1)	0	0	0
Ba(6)	13(1)	13(1)	39(1)	0	0	0
Ba(7)	53(16)	53(16)	70(30)	0	0	0
Mo(l)	8(1)	9(1)	10(1)	−1(1)	0(1)	0(1)
Mo(2)	12(1)	11(1)	13(1)	1(1)	−2(1)	−1(1)
Mo(3)	19(1)	11(1)	9(1)	1(1)	−3(1)	−3(1)
Mo(5)	19(1)	8(1)	11(1)	2(1)	−3(1)	−4(1)
Mo(6)	10(1)	9(1)	10(1)	0(1)	−1(1)	−1(1)
Mo(7)	9(1)	8(1)	11(1)	1(1)	−1(1)	−1(1)

[a] The anisotropic displacement factor exponent takes the form: $-2\pi^2[h^2a^{*2}U11 + \cdots + 2hka^*b^*U12]$.

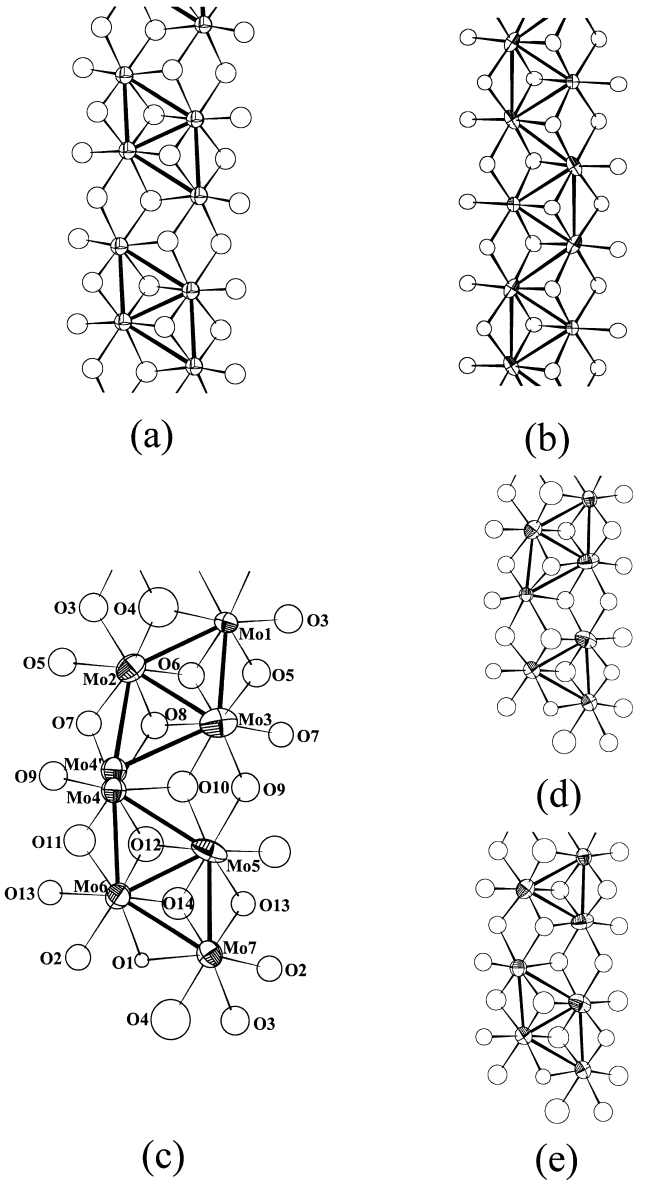

Fig. 4. Sections of the metal-oxide chains in: (a) $K_2Mo_8O_{16}$, (b) $NdMo_6O_{12}$, (c) $Ba_{\sim 8/7}Mo_8O_{16}$, (d) and (e) represent chains in $Ba_{\sim 8/7}Mo_8O_{16}$ when Mo4 and Mo4′ sites are occupied, respectively. Mo–Mo bonds are represented by solid black lines.

3.2. Crystal structure

$Ba_{\sim 8/7}Mo_8O_{16}$ crystallizes in a hollandite-type structure. Consequently, the Mo–O framework of $Ba_{\sim 8/7}Mo_8O_{16}$ consists of double-rutile chains of edge-sharing MoO_6 octahedra with each octahedron sharing four edges with four other neighboring octahedra. These double strings which run parallel to the *c*-axis are then linked together by sharing sp^2-type oxygen-atom corners to form large square tunnels in which the Ba^{2+} ions are located (Fig. 3) as well as smaller empty sized channels similar to those found in the rutile-type structure. As observed in the previous reduced molybdenum oxides crystallizing with a hollandite-type structure, the Mo atoms form Mo–Mo bonds which lead to a clustering of the Mo atoms. Thus tetrameric molybdenum Mo_4 clusters (Fig. 4a) with intracluster distances ranging between 2.53 and 2.84 Å and intercluster distances greater than 3 Å are observed in the $Ba_{1.14}Mo_8O_{16}$ and $K_2Mo_8O_{16}$ compounds while Mo_3 triangles either isolated or forming infinite chains are present in $La_{1.16}Mo_8O_{16}$ [6] and RMo_6O_{12} (i.e. $R_{1.33}Mo_8O_{16}$ R = Pr, Nd) [7] (Fig. 4b), respectively. In $Ba_{\sim 8/7}Mo_8O_{16}$, as the Mo4 and Mo4′ sites can not be occupied simultaneously (Fig. 4c), the Mo atoms in the double edge-sharing rutile-type chains form triangular Mo_3 and planar rhomboidal Mo_4 clusters that coexist in equal proportions (Fig. 4d,e). The Mo–Mo distances range from 2.5341(8) to 2.646(2) A for the Mo_3 triangles occurring with the probability of 71% (site Mo4′ empty) and from 2.5481(9) to 2.696(2) A for the other ones (site Mo4 empty) (Fig. 4d,e). For the Mo_4 rhomboids, the Mo–Mo distances vary from 2.5341(8) to 2.894(4) Å (site Mo4′ full) and from 2.5481(9) to 2.786(3) Å (site Mo4 full). The shortest distance between the triangular Mo_3 and the rhomboidal Mo_4 clusters is 3.047(4) Å and thus is only weakly bonding. The oxygen atoms can be divided into two different types: O2, O3, O5, O7, O9, O11 and O13 which interconnect the double chains and are linked in trigonal planar-like coordination to three Mo atoms, and O1, O4, O6, O8, O10, O12 and O14 which bridge three

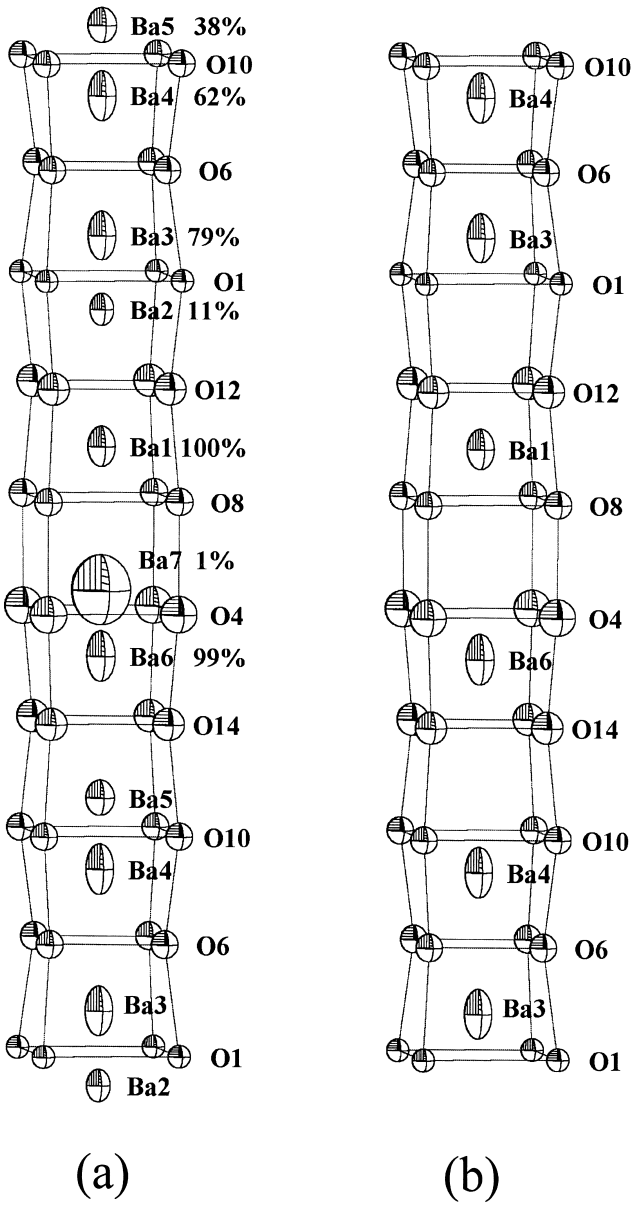

Fig. 5. Views perpendicular to the *c*-axis of $Ba_{\sim 8/7}Mo_8O_{16}$ showing (a) the Ba^{2+} sites and their occupancy within a channel and (b) the most plausible distribution of the Ba^{2+} cations.

Mo atoms of the same double chain and participate to the environment of the Ba^{2+} cation. The Mo–O bond lengths vary from 1.81(1) to 2.481(8) Å. From the Mo–O bond lengths, the valences of the crystallographically independent Mo atoms were calculated by using the relationship of Brown and Wu [$(s = (d_{Mo-O}/1.882)^{-6.0})$] [14]. This yields an average value of +3.73(3), in reasonably good agreement with the expected value of +3.714.

Each barium ion is surrounded by eight intrachain oxygen atoms in a square prismatic arrangement. On average four of the seven possible sites of the 7c supercell along the *c*-axis are occupied by the Ba^{2+} cations. The most plausible Ba^{2+} distribution correspond to the sequence . . . Ba–□–Ba–Ba–□–Ba–□– . . . (□ symbolizes a vacancy) as shown in Fig. 5. The Ba–O distances are in the range 2.51(1)–2.981(8) Å. The distances between two close Ba^{2+} ions are comprised between 3.577(6) and 3.79(4) Å. In comparison, the shortest Ba^{2+}–Ba^{2+} distances in $Ba_{1.13}Mo_8O_{16}$ is 3.34 Å and in $BaRu_6O_{12}$, which also adopts a hollandite structure, 3.86 Å.

In summary, millimeter-size crystals of the new modulated reduced molybdenum oxide $Ba_{\sim 8/7}Mo_8O_{16}$ which crystallizes with a hollandite-related structure have been grown by molten salt electrolysis. The dominant feature of the crystal structure is the formation of triangular Mo_3 and planar rhomboidal Mo_4 clusters that coexist in equal proportions within the Mo_8O_{16} double rutile chains. Band structure calculations would be helpful to understand the different kinds of clustering observed in the reduced molybdenum hollandite-type structures as well as their physical properties.

References

[1] A. Byström, A.M. Byström, Acta Crystallogr. 3 (1950) 146.
[2] A.E. Ringwood, S.E. Kesson, N.G. Ware, W. Hibberson, A. Major, Nature 278 (1979) 219.
[3] E. Fanchon, in: Thesis, Grenoble, France, 1987.
[4] C.C. Torardi, J.C. Calabrese, Inorg. Chem. 23 (1984) 3281.
[5] C.C. Torardi, R.E. McCarley, J. Solid State Chem. 37 (1981) 393.
[6] H. Leligny, Ph. Labbé, M. Ledésert, B. Raveau, C. Valdez, W.H. McCarroll, Acta Crystallogr. B48 (1992) 134.
[7] J. Tortelier, W.H. McCarroll, P. Gougeon, J. Solid State Chem. 136 (1998) 87.
[8] Nonius, in: Collect, Denzo, Scalepack, Sortav. Kappa Ccd Program Package, Nonius BV, Delft, The Netherlands, 1998.
[9] R.H. Blessing, Acta Crystallogr. A51 (1995) 33.
[10] G.M. Sheldrick, in: SHELXS-86, Program for the Solution of Crystal Structures, Univ. of Göttingen, Germany, 1986.
[11] G.M. Sheldrick, in: SHELXS-97, Program For the Refinement of Crystal Structures, Univ. of Göttingen, Germany, 1997.
[12] F.C. Mijlhoff, D.J. Ijdo, H.W. Zandbergen, Acta Crystallogr. B41 (1985) 98.
[13] L.C. Nistor, G. Van Tendeloo, S. Amelinckx, J. Solid State Chem. 109 (1994) 152.
[14] I.D. Brown, K.K. Wu, Acta Crystallogr. B32 (1976) 1957.